Chapter 3
Band-Gap Properties of Prestressed Structures

M. Gei, D. Bigoni, A.B. Movchan, and M. Bacca

Abstract The design of periodic and quasiperiodic structures possessing innovative filtering properties for elastic waves opens the way to the realization of elastic metamaterials. In these structures prestress has a strong influence, 'shifting' in frequency, but also 'annihilating' or 'nucleating' band gaps. The effects of prestress are demonstrated with examples involving flexural waves in periodic and quasiperiodic beams and periodic plates. Results highlight that prestress can be employed as a 'tuning parameter' for continuously changing vibrational properties of elastic metamaterials.

3.1 Introduction

By analogy with their electromagnetic counterpart, 'elastic metamaterials' are designed to become innovative filters for mechanical waves. The design is focussed on vibrational properties connected with the periodicity of a structure, which can be engineered to provide special effects, such as: band gaps (frequency ranges where the waves are evanescent [17, 22, 36, 39]), localized or defect modes (an exponentially localized waveform located near a periodicity-breaking element [2, 30]), negative refraction (refraction occurring on the same side of the normal to the interface where the incoming wave is incident [15, 32, 34, 40, 41]), and effective negative

M. Gei (✉) · D. Bigoni · M. Bacca
Department of Civil, Environmental and Mechanical Engineering, University of Trento, via Mesiano 77, 38123 Trento, Italy
e-mail: massimiliano.gei@unitn.it

D. Bigoni
e-mail: davide.bigoni@unitn.it

M. Bacca
e-mail: mattia.bacca@unitn.it

A.B. Movchan
Department of Mathematical Sciences, University of Liverpool, Liverpool L69 3BX, UK
e-mail: abm@liv.ac.uk

R.V. Craster, S. Guenneau (eds.), *Acoustic Metamaterials*,
Springer Series in Materials Science 166, DOI 10.1007/978-94-007-4813-2_3,

mass effects (corresponding to an exponential decay of vibrational modes, rather than sinusoidal propagation [24, 29, 35]).

Wave propagation within elastic structures is strongly influenced by the pre-existing state of stress, the so-called 'prestress'. This effect is well-known in structural engineering [7, 23, 26–28], in two-dimensional boundary-value problems of prestressed solids [3, 4, 9, 11, 13, 14, 31, 37] and finds simple experimental demonstrations, so that for instance prestress plays a chief role in the vibrational behaviour of stringed musical instruments: in the absence of the strong compression induced by ribs a piano soundboard would not vibrate properly. It is therefore not surprising that prestress can have a determinant influence on dynamical properties of periodic structure, as demonstrated in [5, 12, 33].

Our purpose is to review results by Gei et al. [12] and Gei [10] relative to vibrating periodic and quasiperiodic beams and extending these to vibrating periodic plates. We will show that prestress can: (i.) change the dispersion properties of Floquet-Bloch elastic waves, (ii.) shift the frequency range of band gaps towards high (low) frequency, when tensile (compressive) prestress is applied (iii.) 'annihilate' or (iv.) 'nucleate' band gaps.

For periodic prestressed structures, we will use the Floquet-Bloch technique directly (analytically in the case of beams and numerically in the case of plates), while for the quasiperiodic case the transmission matrix of the elementary cell is obtained, so that applying the Floquet-Bloch conditions a set of eigenvalue problems for the circular frequency is derived. In the case of quasiperiodic beams (generated employing the Fibonacci sequence), flexural waves are considered and the following aspects are analyzed: (i.) the number of stop/pass bands and (ii.) the self-similarity of dispersion diagrams as functions of the generation index i of the elementary cell; (iii.) the role of an invariant function which governs the scaling of stop/pass band structure; and (iv.) the possibility of shifting and broadening the stop/pass bands.

3.2 Band Gaps for Periodic Beams on a Spring Foundation

Floquet-Bloch propagation of flexural waves is investigated within prestressed periodic beams on an elastic 'spring' foundation (so-called 'Winkler type') which models a typical design problem of Microelectromechanical systems (MEMS) technology, namely, vibrations of a relatively stiff elastic layer bonded to a thick elastic layer. The geometry of the problem under consideration is shown in Fig. 3.1, where the period is equal to d and N denotes the constant longitudinal prestress applied at infinity.

We will also consider a perturbation to the periodicity by addition of a mass into the central cell of the structure, as shown in Fig. 3.1(b). This perturbation does not affect the physical characteristics of the other cells and we will show that an exponentially localized wave form will become possible, within a certain frequency range.

The structure is made up of two phases, $m = 1$ and $m = 2$, so that the time-harmonic flexural displacement $w_m(z)$ satisfies the following differential equation (a prime denotes differentiation with respect to the longitudinal coordinate z)

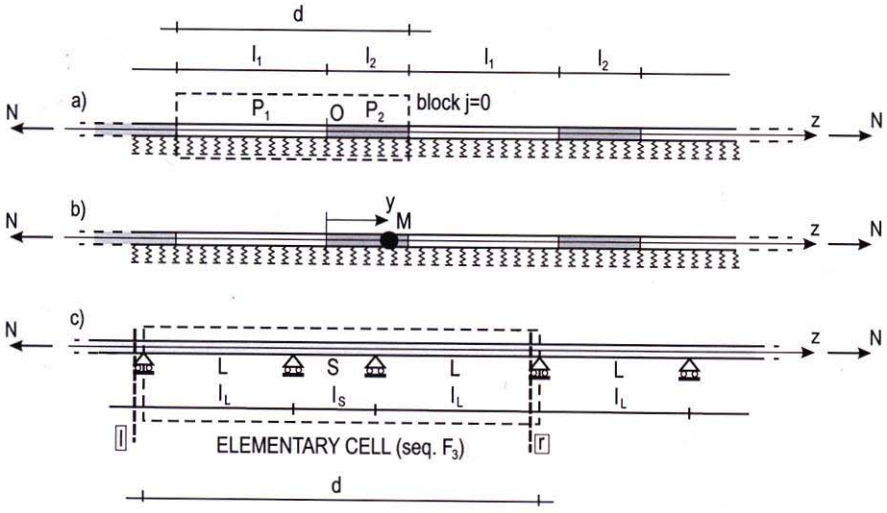

Fig. 3.1 Periodic and quasiperiodic beam systems. (**a**) Piecewise homogeneous beam on an elastic 'spring' foundation; (**b**) same as (**a**), but with an additional mass M placed at $z = y$ to investigate 'band-gap localized modes'; (**c**) quasiperiodic multisupported beam with the elementary cell generated by the Fibonacci sequence F_3. N represents the longitudinal prestress. (**a**), (**b**) are reprinted from [12] with permission [Copyright (2010) American Institute of Physics]. (**c**) is reprinted from [10] with permission from Elsevier. Copyright (2010) American Institute of Physics

$$B_m w_m'''' - N w_m'' + \left(S - \rho_m \omega^2\right) w_m = 0 \quad (m = 1, 2), \tag{3.1}$$

where ρ_m is the piecewise-constant mass density, $B(z) = I(z)E(z)$ the bending stiffness [with the second-order moment $I(z)$ and the Young modulus $E(z)$] and the stiffness of the elastic foundation is denoted by S (see [38] for details).

Note that the bending stiffness $B(z)$ could be easily made dependent on the longitudinal prestress N acting on the beam, a dependency neglected in the following for simplicity.

The solution for flexural displacements is sought in the form

$$w_m = \xi_m \exp\left(i k^{(m)} z\right) \quad (m = 1, 2), \tag{3.2}$$

so that a substitution of (3.2) into (3.1) yields the following equation for the circular frequency ω

$$\left(k^{(m)} r_m\right)^4 + \overline{N}_m \left(k^{(m)} r_m\right)^2 + \overline{S}_m - P_m \omega^2 = 0 \quad (m = 1, 2), \tag{3.3}$$

where the following dimensionless parameters have been introduced

$$\overline{N}_m = \frac{N r_m^2}{B_m}, \qquad \overline{S}_m = \frac{S r_m^4}{B_m} \quad (m = 1, 2), \tag{3.4}$$

in which r_m are the radii of inertia of the beam cross-section, while

$$P_m = \frac{\rho_m r_m^4}{B_m} \quad (m = 1, 2) \tag{3.5}$$

have the dimension of a squared time. The parameters r_m are related to the second-order moments I_m and the cross-sectional areas A_m of the two phases of the beam by

$$r_m = \sqrt{I_m / A_m} \quad (m = 1, 2). \tag{3.6}$$

Equation (3.3) admits eight solutions

$$k^{(m)}_{1,2,3,4} = \pm \frac{1}{r_m} \sqrt{-\frac{\overline{N}_m}{2} \pm \sqrt{\frac{\overline{N}_m^2}{4} + P_m \omega^2 - \overline{S}_m}} \quad (m = 1, 2), \tag{3.7}$$

so that the transverse displacements w_1, w_2 become a linear combination of the following four terms

$$w_1(z) = \sum_{p=1}^{4} \xi_1^p \exp\left(i k_p^{(1)} z\right), \qquad w_2(z) = \sum_{p=1}^{4} \xi_2^p \exp\left(i k_p^{(2)} z\right), \tag{3.8}$$

where the eight constants ξ_1^p and ξ_2^p $(p = 1, \ldots, 4)$ can be obtained by imposing the interface conditions at the internal interface of the elementary block; these are: continuity of displacement, rotation, bending moment and shear force. Therefore, for the block $j = 0$ the interface is located at $z = 0$ and the corresponding interface conditions for the functions w_1, w_2 and their derivatives are

$$\begin{aligned} &w_1(0) = w_2(0), && w_1'(0) = w_2'(0), \\ &B_1 w_1''(0) = B_2 w_2''(0), && B_1 w_1'''(0) = B_2 w_2'''(0), \end{aligned} \tag{3.9}$$

while the remaining four equations follow from the imposition of the *Floquet-Bloch conditions*, linking fields at the boundaries of the elementary block

$$w_2\left(l_2^-\right) = w_1\left(-l_1^+\right) \exp(i K d), \qquad w_2'\left(l_2^-\right) = w_1'\left(-l_1^+\right) \exp(i K d), \tag{3.10}$$

$$B_2 w_2''\left(l_2^-\right) = B_1 w_1''\left(-l_1^+\right) \exp(i K d), \qquad B_2 w_2'''\left(l_2^-\right) = B_1 w_1'''\left(-l_1^+\right) \exp(i K d), \tag{3.11}$$

where K is the Bloch parameter.

The vanishing of the determinant of the matrix associated with (3.9)–(3.11) yields the dispersion equation of the beam system. Note that if ω is taken to be zero in (3.1) and (3.7), the system (3.9)–(3.11) provides the buckling load of the structure [8].

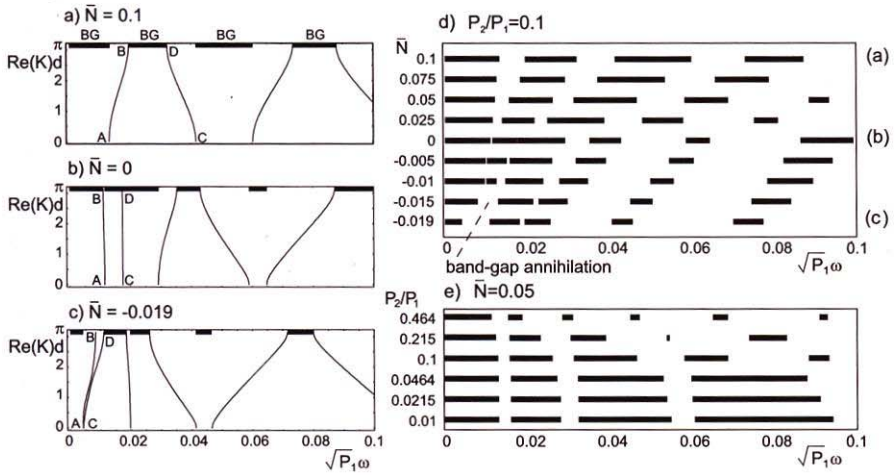

Fig. 3.2 Dispersion diagrams [circular frequency $\sqrt{P_1}\omega$ versus Bloch parameter $\mathrm{Re}(K)d$] and band gap/pass band distribution for a beam on an elastic foundation with piecewise constant mass density [Fig. 3.1(a)] and homogeneous flexural stiffness, $B_1 = B_2$ ($P_2/P_1 = 0.1$, $\overline{S} = 0.0001$, $r/d = 0.015$, $l_1 = l_2 = d/2$). Dispersion diagrams: (**a**) tensile prestress: $\overline{N} = 0.1$; (**b**) null prestress: $\overline{N} = 0$; (**c**) near-buckling ($\overline{N}_{buckl} = -0.02$) compressive prestress: $\overline{N} = -0.019$. BG denotes a band gap. Note that the compressive stress in part (**c**) induces the annihilation of the second band gap (between branches AB and CD). Band gap/pass distribution (**d**) in terms of prestress $\overline{N}$ ($P_2/P_1 = 0.1$); (**e**) in terms of the contrast parameter P_2/P_1 (logarithmic scale) ($\overline{N} = 0.05$). The band-gap annihilation induced by a compressive force is highlighted. Reprinted from [12] with permission. Copyright (2010) American Institute of Physics

3.2.1 Dispersion Diagrams and Band-Gap Shift

The dispersion equation is solved in Fig. 3.2 for the beam sketched in Fig. 3.1(a) (without defects) and with piecewise constant mass density ($\rho_1 \neq \rho_2$), but uniform bending stiffness ($B_1 = B_2$, yielding $\overline{N}_1 = \overline{N}_2 = \overline{N}$). The case $P_2/P_1 = 0.1$, $\overline{S} = 0.0001$, $r/d = 0.015$, $l_1 = l_2 = d/2$, is considered for three different levels of prestress $\overline{N}$ [tensile, null and compressive, in parts (a), (b) and (c), respectively]. For the beam under consideration, the buckling force corresponds to $\overline{N}_{buckl} = -0.02$, while the cutoff frequency of the homogeneous counterpart (which can be recovered if $P_1 = P_2$) is $\sqrt{P_1}\omega_0 = 0.01$.

In general, at a given dimensionless circular frequency $\sqrt{P_1}\omega$, four complex values of the Bloch parameter K can be found from the dispersion equation. In particular, a propagating mode [like those displayed in Figs. 3.2(a), (b), (c)] corresponds to a pure real K, while a monotonic decaying mode is found when K is purely imaginary; for complex conjugate Bloch parameters, the mode also does not propagate and decays, with a sinusoidal decaying. Diagrams displayed in Figs. 3.2(a), (b), (c) are symmetric with respect to the vertical axis $K = 0$, so that only the positive ranges have been plotted. The band gap ('BG') frequency ranges are marked with black segments.

The band-gap distribution is reported as a function of the prestress for fixed contrast parameter $P_2/P_1 = 0.1$ in Fig. 3.2(d), while a fixed, small and tensile prestress is assumed in Fig. 3.2(e), for varying P_2/P_1. The latter figure makes evident that the cutoff region is not strongly influenced by the contrast parameter P_2/P_1, and that the range where the increase in the size of the BG zones is more pronounced occurs for $0.0464 < P_2/P_1 < 0.464$.

Let us consider now the two lower frequency band gaps in Figs. 3.2(a), (b), (c), one of which is present also in a homogeneous beam on an elastic foundation. The prestress strongly modifies the band gap intervals (shifting these toward higher frequencies for tensile loading) and, when this becomes compressive, the higher frequency band gap (between branches AB and CD in Fig. 3.2) is reduced in size and *annihilated already before the buckling load is attained.*

3.3 Band-Gap Localized Defect Modes

A 'band-gap localized defect mode' is a vibration mode associated with a single mass placed along the beam at a frequency within a band gap in the dispersion diagram. The influence of prestress N on those modes is demonstrated for an infinite piecewise uniform beam on an elastic foundation, making use of a Green's function formulation. While for a homogeneous beam on an elastic foundation localized modes available below the cut-off frequency can be computed analytically (see [12]), for a piecewise homogeneous beam the Green's function is not immediately available (although—in principle—it can be obtained analytically), so that we prefer pursuing an approximate calculation, where a 'sufficiently long', but finite, beam (seven elementary cells of length d in our examples) is solved, with a unit force applied at the central cell (the fourth cell in our examples).

The properties of localized modes are very interesting for a piecewise beam as: (i) the dispersion diagrams exhibit several band gaps (not only one as in the uniform case); (ii) the concentrated mass can be placed at different positions within the cell, thus providing different responses; (iii) the vibration modes of the mass can be made more or less localized in the vicinity of the defect depending of the frequency (an effect shown in [30]).

Results pertinent to the seven-cell structure are reported in Fig. 3.3. Here the ranges of frequencies where localized modes associated with the concentrated mass are possible are reported as functions of the position y (normalized through division by d) of the mass in the central cell, for two levels of prestress, namely, $\overline{N} = 0.025$ in Fig. 3.3(a) and $\overline{N} = 0$ in Fig. 3.3(b).

In both parts (a) and (b) of Fig. 3.3 the first three band gaps have been investigated, placing masses at discrete distances multiple of $d/20$. Results depend on the dimensionless frequencies $\sqrt{P_1}\omega$, to generate localized modes associated with $\overline{M} = 1$ (denoted with black dots) and 10 (denoted with black squares), where the dimensionless concentrated mass $\overline{M}$ is defined now with respect to the mass density and radius of inertia of part 1, namely,

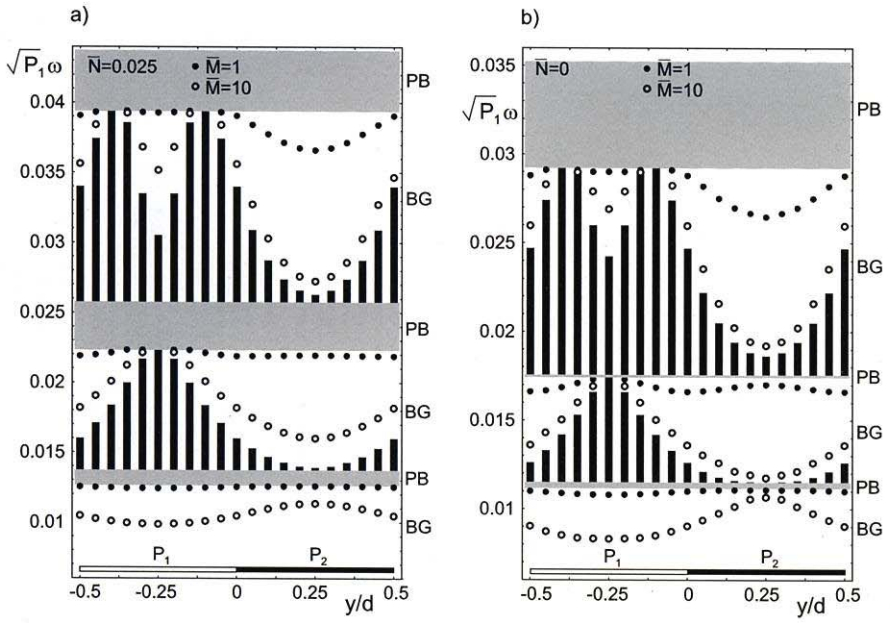

Fig. 3.3 Dimensionless frequency $\sqrt{P_1}\omega$ at which a localized mode connected to a concentrated point mass located at y [Fig. 3.1(b)] exists for $\overline{M} = 1$ (*black dots* in the figure) and $\overline{M} = 10$ (*open circles*) (the following values of constants have been taken: $P_2/P_1 = 0.1$, $l_1 = l_2 = d/2$, $r/d = 0.015$, $\overline{S} = 0.0001$). (**a**) Tensile prestress: $\overline{N} = 0.025$; (**b**) null prestress: $\overline{N} = 0$. BG denotes a band gap, PB a pass band (see Fig. 3.2). A *black vertical segment* in the band-gap zone indicates a frequency range where localized modes are not possible. Reprinted from [12] with permission. Copyright (2010) American Institute of Physics

$$\overline{M} = \frac{M}{2\rho_1 r_1}. \tag{3.12}$$

The black vertical segments crossing the band gaps indicate frequency ranges where *localized modes (and effective negative mass effects) cannot be generated just by inserting a single concentrated mass*, being the displacement of the point of application of the unit force out of phase with respect to the force itself. We note that at certain locations y/d within the second and third band gap these vertical segments cross the entire range (for instance at $y = 0.25d$, within the second band gap, and at $y = 0.2d, 0.8d$, within the third band gap), so that *in these cases localized modes cannot be obtained for an applied finite and positive concentrated mass.*

3.4 Periodic Plates Under Tensile Prestress

Wave propagation in two-dimensional structures becomes more complicated, but more interesting, than propagation in beam elements. We address transversal vibration of infinite and periodic Kirchhoff plates, prestressed with tensile forces, and we

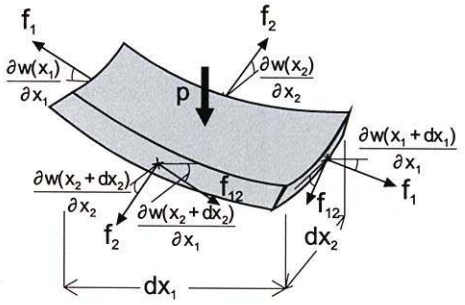

Fig. 3.4 An element of a prestressed elastic Kirchhoff plate, subject to a transversal dead load p and displacement w. The prestress has normal components f_1 and f_2 and shearing component f_{12}

will show that the prestress can induce anisotropy effects that, 'added' to effects associated with the periodicity, can create privileged propagation directions as related to the presence of 'directional' band gaps. Note that a two-dimensional plate model provides an accurate approximation only for the lower-frequency modes, while correct computations at high-frequency would require a model of Mindlin plate, or a fully three-dimensional analysis.

With reference to Fig. 3.4, the differential equations governing dynamics of an elastic Kirchhoff plate of thickness h, prestressed through two normal f_1 and f_2 and shearing f_{12} tractions, are

$$B\nabla^4 w - f_1\frac{\partial^2 w}{\partial x_1^2} - f_2\frac{\partial^2 w}{\partial x_2^2} - 2f_{12}\frac{\partial^2 w}{\partial x_1 \partial x_2} = -\rho h\ddot{w} + p, \tag{3.13}$$

where w is the transversal displacement, ρ is the mass density per unit volume, p the transversal dead load, a superimposed dot means time-derivative, and B is the flexural rigidity, which can be related to the elastic modulus E, the Poisson's coefficient ν of the material, and the thickness of the plate h as

$$B = \frac{Eh^3}{12(1-\nu^2)}. \tag{3.14}$$

Assuming that the shearing component of the prestress is null, $f_{12} = 0$, the time-harmonic free oscillations are ruled by the equation

$$B\nabla^4 w - \rho h\omega^2 w - f_1\frac{\partial^2 w}{\partial x_1^2} - f_2\frac{\partial^2 w}{\partial x_2^2} = 0, \tag{3.15}$$

where ω is the circular frequency. Equation (3.15) holds at every point of the domain Ω defining the plate. A weak formulation of dynamics of a plate can be obtained transforming (3.15) into

$$\int_{\Omega^*} (\boldsymbol{\chi}\cdot\boldsymbol{C}\boldsymbol{\chi})\, d\Omega^* - \rho h\omega^2 \int_{\Omega^*} w^2\, d\Omega^* - \int_{\Omega^*}\left[f_1\left(\frac{\partial w}{\partial x_1}\right)^2 + f_2\left(\frac{\partial w}{\partial x_2}\right)^2\right] d\Omega^* = 0, \tag{3.16}$$

holding for every subdomain Ω^* of Ω, in which

$$\boldsymbol{\chi} = \left(\frac{\partial^2 w}{\partial x_1^2}, \frac{\partial^2 w}{\partial x_2^2}, \frac{\partial^2 w}{\partial x_1 \partial x_2} \right)^T, \qquad \boldsymbol{C} = B \begin{pmatrix} 1 & \nu & 0 \\ \nu & 1 & 0 \\ 0 & 0 & (1-\nu)/2 \end{pmatrix}. \tag{3.17}$$

A finite element discretization of the domain Ω is now introduced through the shape functions (collected into the row vector $\boldsymbol{\Phi}$), so that the transversal displacement and the rotation can be expressed as

$$w = \boldsymbol{\Phi} \cdot \boldsymbol{u}^e, \tag{3.18}$$

where $\boldsymbol{u}^e$ is the vector collecting the nodal displacements and rotations of the eth element.

Using (3.18) in $(3.17)_1$, we obtain

$$\boldsymbol{\chi} = \boldsymbol{D}\boldsymbol{u}^e, \qquad \frac{\partial w}{\partial x_1} = \frac{\partial \Phi}{\partial x_1}\boldsymbol{u}^e, \qquad \frac{\partial w}{\partial x_2} = \frac{\partial \Phi}{\partial x_2}\boldsymbol{u}^e, \tag{3.19}$$

three equations holding in the domain of the eth element, in which

$$\boldsymbol{D} = \left(\frac{\partial^2 \boldsymbol{\Phi}^T}{\partial x_1^2}, \frac{\partial^2 \boldsymbol{\Phi}^T}{\partial x_2^2}, \frac{\partial^2 \boldsymbol{\Phi}^T}{\partial x_1 \partial x_2} \right)^T. \tag{3.20}$$

If we substitute (3.19) into (3.16) and identify Ω^* with the domain of the eth element Ω^e, we obtain the eigenvalue problem governing time-harmonic vibration of a finite element

$$\boldsymbol{u}^e \cdot \left(\boldsymbol{K}_e + \boldsymbol{K}_{fe} - \omega^2 \boldsymbol{M}_e \right) \boldsymbol{u}^e = 0, \tag{3.21}$$

where, for the eth elements, $\boldsymbol{M}_e$ is the mass matrix, $\boldsymbol{K}_e$ is the stiffness matrix, while $\boldsymbol{K}_{fe}$ keeps into account the effect of the prestress. Their expressions are

$$\begin{aligned} \boldsymbol{M}_e &= \int_{\Omega^e} \rho h \boldsymbol{\Phi} \boldsymbol{\Phi}^T \, d\Omega^e, \\ \boldsymbol{K}_e &= \int_{\Omega^e} \boldsymbol{D}^T \boldsymbol{C} \boldsymbol{D} \, d\Omega^e, \\ \boldsymbol{K}_{fe} &= \int_{\Omega^e} \boldsymbol{D}_f \cdot \boldsymbol{C}_f \boldsymbol{D}_f \, d\Omega^e, \end{aligned} \tag{3.22}$$

where

$$\boldsymbol{D}_f = \left(\boldsymbol{\Phi}^T, \frac{\partial \boldsymbol{\Phi}^T}{\partial x_1}, \frac{\partial \boldsymbol{\Phi}^T}{\partial x_2} \right)^T, \qquad \boldsymbol{C}_f = \begin{pmatrix} 0 & 0 & 0 \\ 0 & f_1 & 0 \\ 0 & 0 & f_2 \end{pmatrix}. \tag{3.23}$$

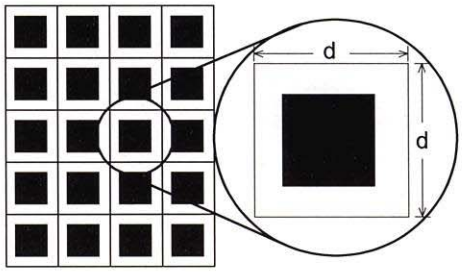

Fig. 3.5 The periodic plate analyzed in the examples. Inclusions are marked black and will be identified with an elastic material less stiff, but heavier, than the matrix

Applying (3.21) to the whole domain Ω of the plate and assembling the matrix of the finite elements, we obtain the mass matrix and the stiffness matrix of the whole cell,

$$\boldsymbol{M} = \sum_e \boldsymbol{M}_e, \qquad \boldsymbol{K} = \sum_e \boldsymbol{K}_e, \qquad \boldsymbol{K}_f = \sum_e \boldsymbol{K}_{fe}, \tag{3.24}$$

where $\boldsymbol{M}_e$, $\boldsymbol{K}_e$ and $\boldsymbol{K}_{fe}$ are the expanded matrices of the element, so that we finally arrive at the eigenvalue problem governing time-harmonic vibrations of the discretized plate

$$\boldsymbol{u} \cdot \left(\boldsymbol{K} + \boldsymbol{K}_f - \omega^2 \boldsymbol{M}\right)\boldsymbol{u} = 0, \tag{3.25}$$

where $\boldsymbol{u}$ is the vector collecting the nodal displacements and rotations of the whole cell.

The Floquet-Bloch condition for a cell of a periodic system made up of square cells of edge d (Fig. 3.5) can be written in terms of transverse displacement w as

$$w(x_1 + md, x_2 + nd) = w(x_1, x_2)e^{i(k_1 md + k_2 nd)}, \tag{3.26}$$

where m and n are integers indexing a node of the cell lattice and $\boldsymbol{k} = (k_1, k_2)$ is the Bloch vector. Note that (3.26) imposes also periodicity restrictions on rotations (and consequently on bending moments and shearing forces).

Using the finite element technique, only one cell is analyzed, so that condition (3.26) has to be imposed on its boundary, where it becomes

$$\begin{aligned} u(d, x_2) &= u(0, x_2)e^{ik_1 d}, \quad 0 \le x_2 \le d, \\ u(x_1, d) &= u(x_1, 0)e^{ik_2 d}, \quad 0 \le x_1 \le d, \end{aligned} \tag{3.27}$$

expressed in terms of generalized displacements (displacements and rotations).

Condition (3.27) imposes a linear dependence between some components of the generalized displacement vector $\boldsymbol{u}$, so that we assume that the linearly independent components $\tilde{\boldsymbol{u}}$ of displacement along the boundary of the periodicity cell can be written as

$$\boldsymbol{u} = \boldsymbol{T}(\boldsymbol{k})\tilde{\boldsymbol{u}}, \tag{3.28}$$

and therefore the eigenvalue problem (3.25) takes the final form

$$\left(\widetilde{\boldsymbol{K}} + \widetilde{\boldsymbol{K}}_f - \omega^2 \widetilde{\boldsymbol{M}}\right)\tilde{\boldsymbol{u}} = 0, \tag{3.29}$$

where

$$\widetilde{\boldsymbol{K}} = \boldsymbol{T}(\boldsymbol{k})^T \boldsymbol{K} \boldsymbol{T}(\boldsymbol{k}), \qquad \widetilde{\boldsymbol{K}}_f = \boldsymbol{T}(\boldsymbol{k})^T \boldsymbol{K}_f \boldsymbol{T}(\boldsymbol{k}), \qquad \widetilde{\boldsymbol{M}} = \boldsymbol{T}(\boldsymbol{k})^T \boldsymbol{M} \boldsymbol{T}(\boldsymbol{k}). \tag{3.30}$$

The eigenvalue problem (3.29) can be numerically solved (we have used Matlab R2007b©). In a dimensionless form, (3.29) becomes

$$\left(\boldsymbol{K}^* + \Xi \boldsymbol{K}_f^* - \widetilde{\omega}^2 \boldsymbol{M}^*\right)\tilde{\boldsymbol{u}} = 0, \tag{3.31}$$

where $\boldsymbol{K}_f^*$ depends on the dimensionless ratio f_2/f_1, while

$$\Xi = \frac{f_1 d^2}{h^3 E}, \qquad \widetilde{\omega} = \frac{d^2}{h}\sqrt{\frac{\rho}{E}}\omega. \tag{3.32}$$

Examples of dispersion diagrams, calculated through solution of the eigenvalue problem (3.31), are reported in Figs. 3.6 and 3.7, where the inclusions have been taken of square shape (as sketched in Fig. 3.5), with an area equal to 0.36 d^2, a stiffness and density contrast respectively equal to $E_{matrix}/E_{inclusion} = 100$ and to $\rho_{matrix}/\rho_{inclusion} = 1/100$.

The dimensionless frequency $\widetilde{\omega}/(2\pi)$ is plotted

- for Fig. 3.6, which refers to the case of isotropic prestress $f_1 = f_2 = f$, along the right-handed triangle ΓMX, with vertices at $\Gamma = (0, 0)$, $M = (\pi, 0)$ and $X = (\pi, \pi)$, see the inset in the figure;
- for Fig. 3.7, which refers to the case of uniaxial prestress $f_2 = 0$, along the right-handed square ΓMXN, with vertices at $\Gamma = (0, 0)$, $M = (\pi, 0)$, $X = (\pi, \pi)$, and $N = (0, \pi)$, see the inset in the figure.

Note that there are, say, 'complete' and 'partial' band gaps, so that the former correspond to grey rectangles crossing completely Figs. 3.6 and 3.7, while the latter only extend to an edge of the triangle ΓMX or of the square ΓMXN. A partial band gap means that there is only a limited angular range of wave propagation direction, while other directions are forbidden within a certain range of frequencies. The presence of a partial band gap can exploited to design special vibrational characteristics. Our results presented in Figs. 3.6 and 3.7 indicate that the global and partial band gaps are strongly influenced by the prestress, so that they can be (i.) shifted in frequency (towards high frequency for tensile prestress), (ii.) reduced or enlarged in size, (iii.) annihilated or (iv.) nucleated.

We can note the different role played by prestress in Fig. 3.6 (where the prestress state is isotropic) and in Fig. 3.7 (where the prestress state is anisotropic), so that for anisotropic (isotropic) prestress there is a progressive reduction (increase) in the number of band gaps, related to the increase in the tensile prestress, so that one complete band gap is nucleated in Fig. 3.6 and one is annihilated in Fig. 3.7.

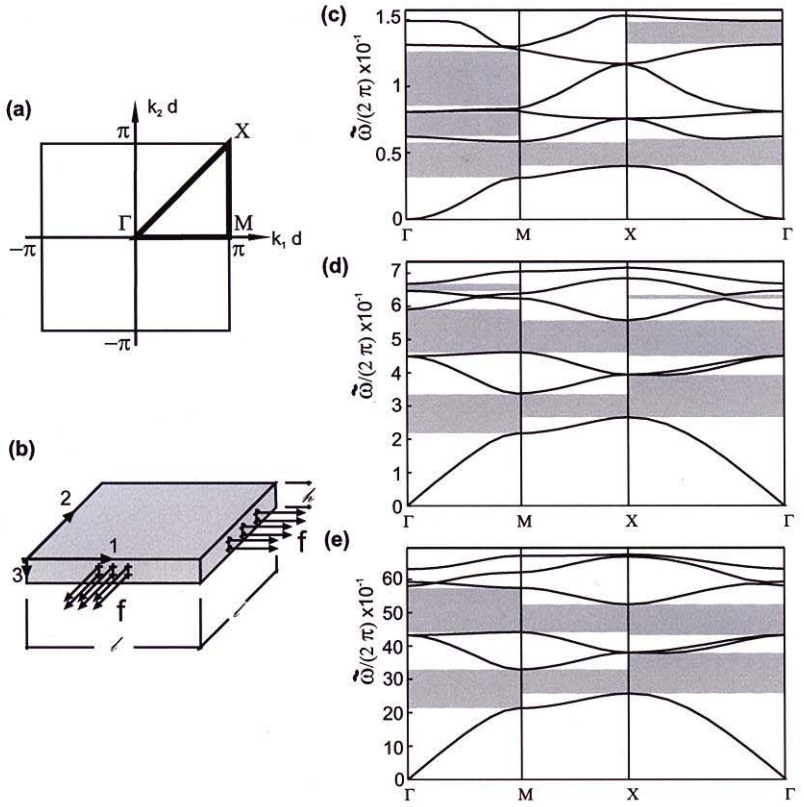

Fig. 3.6 A prestressed plate with an isotropic tensile prestress in the x_1–x_2 plane, so that $f_1 = f_2 = f$. (**a**) the First Irreducible Brillouin Zone; (**b**) the prestressed plate. Dispersion curves of the periodic plate at different values of the prestress f: (**c**) null prestress, $f = 0$; (**d**) moderate prestress, $f = Eh^3/d^2$; and (**e**) high prestress, $f = 10^2 Eh^3/d^2$. The *grey zones* identify the band gaps; note the difference between 'complete' (extending along ΓMX) and'partial' band gaps

Moreover, we see from Fig. 3.7 that there are a number of partial band gaps along the ΓM (the $N\Gamma$) direction that are annihilated (are nucleated) at increasing prestress.

An anisotropy effect related to the prestress is visible in Fig. 3.7, where only the band gaps in the direction of the prestress are annihilated. This effect is important, since we can exploit it to create a waveguide operating in a specific frequency range and controlling the vibration direction, as sketched in Fig. 3.8, where the vibration of a point-source is channelled along a certain direction, tuned by prestress.

3.5 Band Gaps and Self-Similarity in Quasiperiodic Beams

We consider now flexural vibrations of a quasiperiodic multisupported infinite beam. Structures analyzed in this section are formed by a set of—typically two—

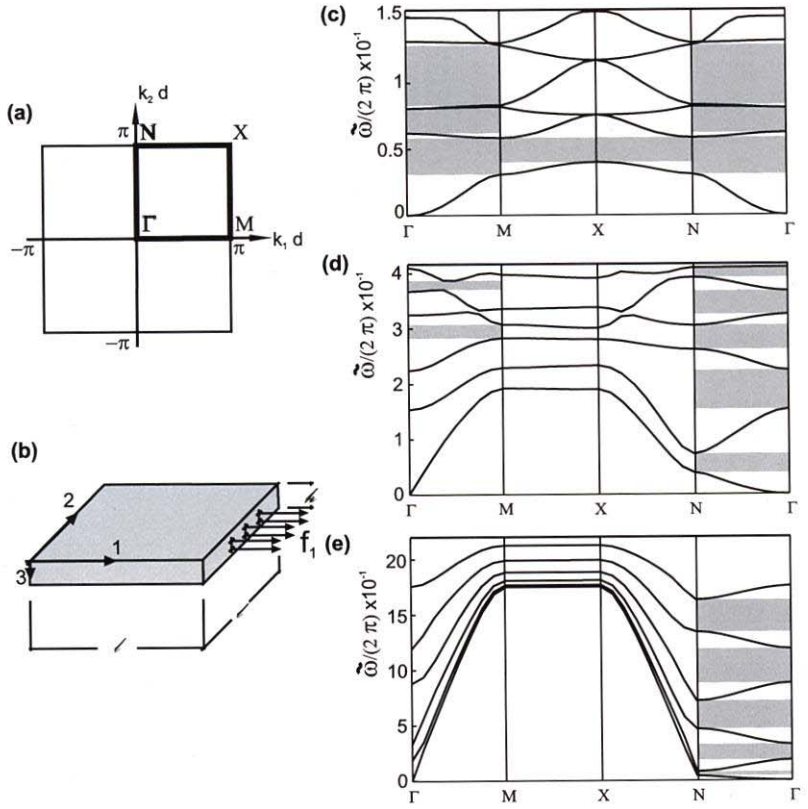

Fig. 3.7 A prestressed plate under a tensile prestress aligned parallel to the x_1-axis. (**a**) The First Irreducible Brillouin Zone; (**b**) the prestressed plate. Dispersion curves of the periodic plate at different values of uniaxial prestress f_1: (**c**) null prestress, $f_1 = 0$; (**d**) moderate prestress, $f_1 = Eh^3/d^2$; and (**e**) high prestress, $f_1 = 10^2 Eh^3/d^2$. The *grey zones* identify the band gaps; note the difference between 'complete' (extending along ΓMXN) and'partial' band gaps

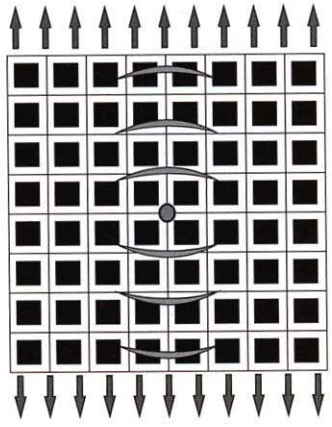

Fig. 3.8 Sketch of a wave guide effect created by prestress and periodicity. Vibrations induced by a pulsating force within a given frequency range are 'channelled' along a privileged direction, set by the prestress

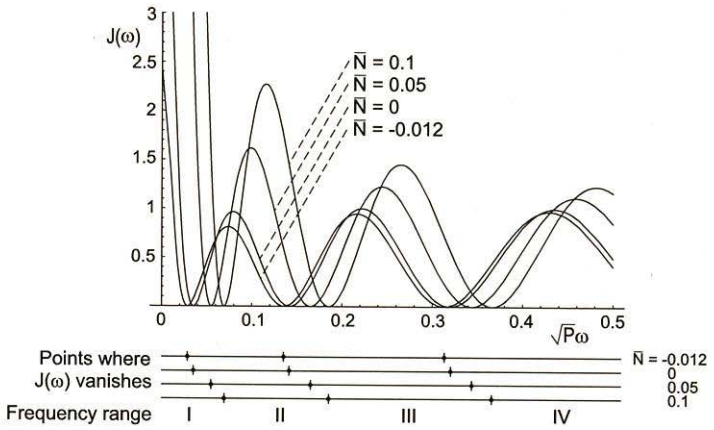

Fig. 3.9 Plots of the invariant $J(\omega)$, (3.46), for different prestress values $\overline{N}$ (for $l_S = l_L/2$). Frequency ranges set by null points of $J(\omega)$ are highlighted. Reprinted from [10] with permission from Elsevier

homogeneous parts combined to create a one-dimensional quasicrystalline pattern such as the Fibonacci sequence (other generation rules do exist, see e.g. the Thue-Morse sequence [25]) and subjected to an axial prestress. The goal is to extend to the domain of structural systems the features of phononic quasiperiodic crystals (see, e.g., [1, 6, 16, 18]). We refer to [10] for more details on the problem.

The elementary cell (Fig. 3.1(c)) of the structure is generated placing the supports at relative distances such that they follow a Fibonacci sequence. Introducing the notation $F_0 = (S)$, $F_1 = (L)$, where S ('short') and L ('long') identify two segments, the Fibonacci sequence obeys the recursive rule $F_i = (F_{i-1}F_{i-2})$ $(i \geq 2)$, where i is the *generation index*, so that $F_2 = (LS)$, $F_3 = (LSL)$ and so on. The number of elements of F_i is equal to $n_i = n_{i-1} + n_{i-2}$ $(i \geq 2, n_0 = n_1 = 1)$, with $\lim_{i\to\infty} n_{i+1}/n_i = \phi$, where ϕ represents the golden ratio $[\phi = (\sqrt{5}+1)/2]$.

The beam is homogeneous, with bending stiffness denoted by B and subjected to a constant prestress N, so that the equation governing transverse displacements $w(z)$ in the harmonic problem is

$$Bw'''' - Nw'' - \rho\omega^2 w = 0. \tag{3.33}$$

The solution can be sought in the form $w(z) = C\exp(ikz)$, yielding the characteristic equation

$$(kr)^4 + \overline{N}(kr)^2 - P\omega^2 = 0, \tag{3.34}$$

where r is the radius of inertia of the cross section and, as in the previous problem,

$$\overline{N} = \frac{Nr^2}{B}, \qquad P = \frac{\rho r^4}{B}. \tag{3.35}$$

Equation (3.34) provides four solutions k, namely

$$k_{1,2} = \pm\frac{1}{r}\sqrt{-\frac{\overline{N}}{2} + \sqrt{\frac{\overline{N}^2}{4} + P\omega^2}}, \qquad k_{3,4} = \pm\frac{1}{r}\sqrt{-\frac{\overline{N}}{2} - \sqrt{\frac{\overline{N}^2}{4} + P\omega^2}}, \tag{3.36}$$

which allow to build the general integral of (3.33) and where the first index is associated with sign '+'.

The dispersion diagram will be obtained through the concept of transmission matrix $\boldsymbol{M}_i$ of the elementary cell (relative to the sequence F_i), which relates the characteristic kinematical quantities of the cell evaluated on the two boundaries. In our case, we note that the configuration of the beam is defined once the rotation $\varphi(z)$ and its derivative $\varphi'(z)$ at each constrained point are known (see Fig. 3.1(c)). Then, we can write formally

$$\boldsymbol{V}_r = \boldsymbol{M}_i \boldsymbol{V}_l, \tag{3.37}$$

where $\boldsymbol{V}_j = [\varphi_j \quad \varphi'_j]^T$ and subscripts r and l denote the right-hand and left-hand boundary of the elementary cell, respectively. The matrix $\boldsymbol{M}_i$ can be assembled multiplicating the matrices of receptances ($\boldsymbol{M}^X$, $X \in \{L, S\}$) associated with all spans within the elementary cell, [10], namely

$$\boldsymbol{M}_i = \prod_{p=1}^{n_i} \boldsymbol{M}^X, \tag{3.38}$$

where $\boldsymbol{M}^X$ is given by

$$\boldsymbol{M}^X = \begin{bmatrix} \frac{\psi^X_{bb}}{\psi^X_{ab}} & \psi^X_{ba} - \frac{\psi^X_{bb}\psi^X_{aa}}{\psi^X_{ab}} \\ \frac{1}{\psi^X_{ab}} & -\frac{\psi^X_{aa}}{\psi^X_{ab}} \end{bmatrix}. \tag{3.39}$$

The entries of the matrix can be calculated from

$$\psi^X_{aa} = \frac{k_1 \cot(k_1 l_X) - k_3 \cot(k_3 l_X)}{k_3^2 - k_1^2}, \qquad \psi^X_{bb} = \frac{k_1 \cot(k_1 l_X) - k_3 \cot(k_3 l_X)}{k_1^2 - k_3^2}, \tag{3.40}$$

$$\psi^X_{ab} = \frac{k_1 \mathrm{cosec}(k_1 l_X) - k_3 \mathrm{cosec}(k_3 l_X)}{k_1^2 - k_3^2}, \qquad \psi^X_{ba} = \frac{k_1 \mathrm{cosec}(k_1 l_X) - k_3 \mathrm{cosec}(k_3 l_X)}{k_3^2 - k_1^2}, \tag{3.41}$$

that depend on circular frequency and prestress N through k_1 and k_3 [see (3.36)].

Transmission matrices $\boldsymbol{M}_i$ have some important properties that can be exploited in the analysis of quasiperiodic structures:

- they follow the recursion rule $\boldsymbol{M}_{i+1} = \boldsymbol{M}_{i-1}\boldsymbol{M}_i$, with $\boldsymbol{M}_0 = \boldsymbol{M}^S$ and $\boldsymbol{M}_1 = \boldsymbol{M}^L$;
- they are unimodular, i.e. $\det \boldsymbol{M}_i = 1$, so that writing down the trace of the equation

$$\boldsymbol{M}_{i+1} + \boldsymbol{M}_{i-2}^{-1} = \boldsymbol{M}_{i-1}\boldsymbol{M}_i + \boldsymbol{M}_{i-1}\boldsymbol{M}_i^{-1},$$

we obtain that the half trace $y_i = \mathrm{tr}\boldsymbol{M}_i/2$ follows the recursive rule [19]

$$y_{i+1} = 2y_i y_{i-1} - y_{i-2}, \tag{3.42}$$

with initial conditions $y_0 = \mathrm{tr}M^S/2$, $y_1 = \mathrm{tr}M^L/2$, $y_2 = \mathrm{tr}(M^S M^L)/2$.

The Bloch-Floquet condition requires that $\boldsymbol{V}_r = \exp(iK)\boldsymbol{V}_l$, so that, combining this with (3.37), the dispersion equation takes the form

$$\left|\boldsymbol{M}_i - \exp(iK)\boldsymbol{I}\right| = 0, \tag{3.43}$$

or

$$K = \arccos\left(\frac{\mathrm{tr}\boldsymbol{M}_i}{2}\right), \tag{3.44}$$

that is a real quantity if $|\mathrm{tr}\boldsymbol{M}_i/2| \leq 1$.

3.5.1 Dispersion Diagrams and Distribution of Pass Bands and Band Gaps

Dispersion diagrams and stop/pass band distributions are now illustrated in terms of dimensionless quantities for $l_S = l_L/2$. An invariant function similar to that introduced by Kohmoto et al. [19] (used to analyze certain solutions of the Schrödinger equation in the presence of quasiperiodic potentials), and employed in [21] to investigate the transmission properties of photonic crystals, can help in the understanding of their properties. Since the recursion rule (3.42) is satisfied, it can be shown [19] that the following quantity is independent of the index i

$$J(\omega) = y_{i+1}^2 + y_i^2 + y_{i-1}^2 - 2y_{i+1}y_i y_{i-1} - 1. \tag{3.45}$$

The explicit expression for $J(\omega)$ turns out to be

$$\begin{aligned} J(\omega) = {} & \frac{k_1^2 k_3^2}{[k_3\sin(k_1 l_L) - k_1\sin(k_3 l_L)]^2[k_3\sin(k_1 l_S) - k_1\sin(k_3 l_S)]^2} \\ & \times \left\{\sin(k_1 l_L)\sin(k_3 l_L)\left[1 - \cos(k_1 l_S)\cos(k_3 l_S)\right]\right. \\ & \left. + \sin(k_1 l_S)\sin(k_3 l_S)\left[\cos(k_1 l_L)\cos(k_3 l_L) - 1\right]\right\}^2, \end{aligned} \tag{3.46}$$

which is a modulated periodic function, sketched in Fig. 3.9 for four different values of the dimensionless prestress $\overline{N}$. The function $J(\omega)$ is identically null for $l_L = l_S$,

which corresponds to the case of a beam resting on equidistant supports. In Fig. 3.9 we have also reported the ranges of frequencies comprised between two null points of the function for different prestresses $\overline{N}$. In particular, the second range will be considered later on.

Single dispersion diagrams for different generation sequences are displayed in Figs. 3.10(a) and 3.10(b) which display cut-off frequencies associated with the discrete distribution of supports. Ranges set by null values of the invariant $J(\omega)$ (Fig. 3.9) are reported to facilitate the analysis of the different cases. Assuming an elementary cell built according to the sequence F_i, in the first range ($0 < \sqrt{P}\omega < 0.03553$ for $\overline{N} = 0$) the number of stop and pass bands equals n_i, while in all other intervals it corresponds to n_{i+1}. In Fig. 3.10(c), the global dispersion diagram combining solutions relative to problems where the elementary cell is generated by sequences F_0 to F_7 is reported. It is interesting to note that the various branches of single diagrams localize within certain ranges of frequencies and stop bands common to all F_i's emerge. The position of these common stop bands is therefore a characteristic of the Fibonacci sequence and can be controlled by changing the ratio l_S/l_L and the space between supports.

The distribution of pass bands follows a self-similar law when the index i of the generation sequence F_i increases. This property can be recognized looking at the rectangular boxes in Fig. 3.11. Here the second frequency range (for which $0.03553 < \sqrt{P}\omega < 0.14212$) is investigated in detail. All rectangles enclose a number of pass bands that, starting from the top, follows the Fibonacci recursion rule: 1, 1, 2, 3, ... However, differently from the axial-wave problem addressed in [10], the relative positions of pass bands with respect to those of the preceding row strongly change, depending on their position on the spectrum.

The function $J(\omega)$ controls also the scaling of pass-band widths changing the sequence F_i. In quantum mechanics, Kohmoto and Oono [20] established that the ratio between the widths of two pass bands (F_i and F_{i+3}, $\forall i$) centered at the same frequency is given by the factor $f(\omega)$, which depends on $J(\omega)$ through the relationship

$$f(\omega) = \sqrt{1 + 4\big[J(\omega) + 1\big]^2} + 2\big[1 + J(\omega)\big]. \tag{3.47}$$

Compared to the case investigated by Kohmoto and Oono, where $J(\omega)$ was a constant, here f depends on ω, however its role in setting the scaling remains essentially the same. The function $f(\omega)$ is sketched in Fig. 3.12(a) for four values of $\overline{N}$. Denoting by $q_k(F_i)$ the width of the pass band for F_i at a frequency corresponding to the index k, f describes exactly their scaling, namely the ratio $q_k(F_i)/q_k(F_{i+3})$, only when the generation index i is relatively high, as shown in Fig. 3.12(b) for two cases (for $\sqrt{P}\omega = 0.060$, $k = 1$, and 0.0956, $k = 2$).

The self-similarity properties show that periodic structures built with a quasiperiodic elementary cell can display very narrow stop and pass bands and therefore can be exploited, in principle, to conceive very sensitive filters.

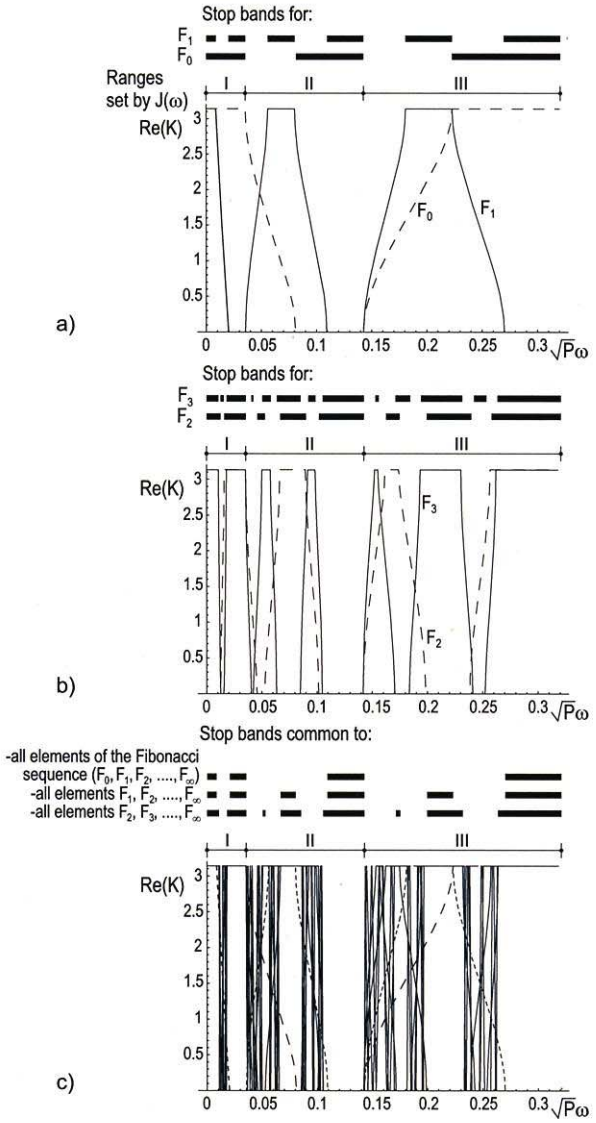

Fig. 3.10 Dispersion diagrams for flexural waves for beams generated by elementary cells given by sequences (**a**) F_0 and F_1, (**b**) F_2 and F_3; (**c**) global dispersion diagram for beams generated by elements F_i ($i = 0, \ldots, 7$) and stop bands common to all elements of the Fibonacci sequence (frequency intervals where waves cannot propagate in any structure generated by a generic F_i with $i = 0, \ldots, \infty$), to all elements F_i with $i = 1, \ldots, \infty$, and to all elements F_i with $i = 2, \ldots, \infty$; *long-dashed line*: solutions for F_0; *short-dashed line*: solutions for F_1; *solid lines*: cumulated diagram for cases F_2 to F_7. In all plots $l_S = l_L/2$ and $\overline{N} = 0$. Reprinted from [10] with permission from Elsevier

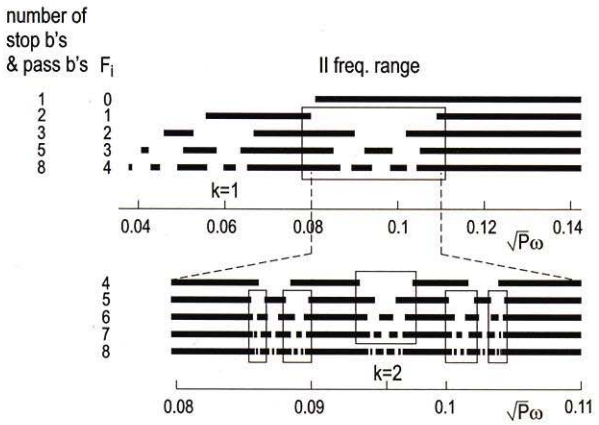

Fig. 3.11 Stop-band structure in the second frequency range ($0.03553 < \sqrt{P}\omega < 0.14212$, see Fig. 3.10) for beams generated by sequences F_0 to F_8, for $l_S = l_L/2$ and $\overline{N} = 0$. Indices k's identify the values of the dimensionless frequency $\sqrt{P}\omega = 0.06$ ($k = 1$) and 0.0956 ($k = 2$) (see Fig. 3.12). All rectangles contain the same self similar, recursive band structure. Reprinted from [10] with permission from Elsevier

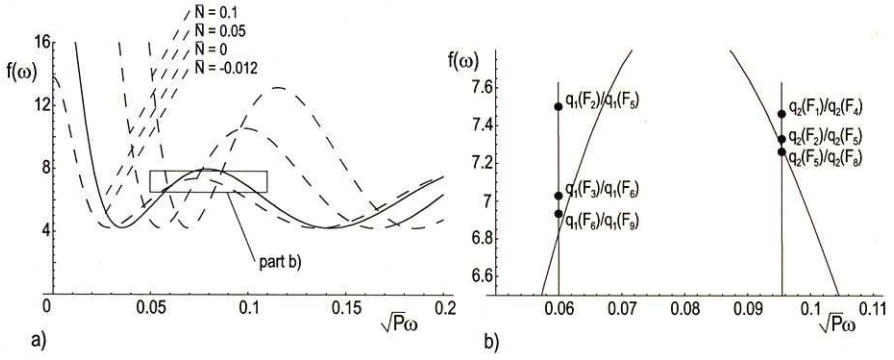

Fig. 3.12 Function $f(\omega)$ (3.47) describing the scaling factor of pass-band widths between F_i and F_{i+3} for the flexural problem. In part (**b**), the plot of $f(\omega)$ for $\overline{N} = 0$ is reported (*solid line*) and the scaling is verified for pass bands at $\sqrt{P}\omega = 0.060$ ($k = 1$, see Fig. 3.11) and at $\sqrt{P}\omega = 0.0956$ ($k = 2$). In both cases the relevant value of f describes the pass-band width scaling $q_k(F_i)/q_k(F_{i+3})$ at high index i. Reprinted from [10] with permission from Elsevier

3.5.2 Effect of the Prestress

We want to explore now how the prestress affects the positions of stop and pass bands in the dispersion diagram for flexural waves of a quasiperiodic, multisupported beam. We note that under compression the structure can buckle at a load that

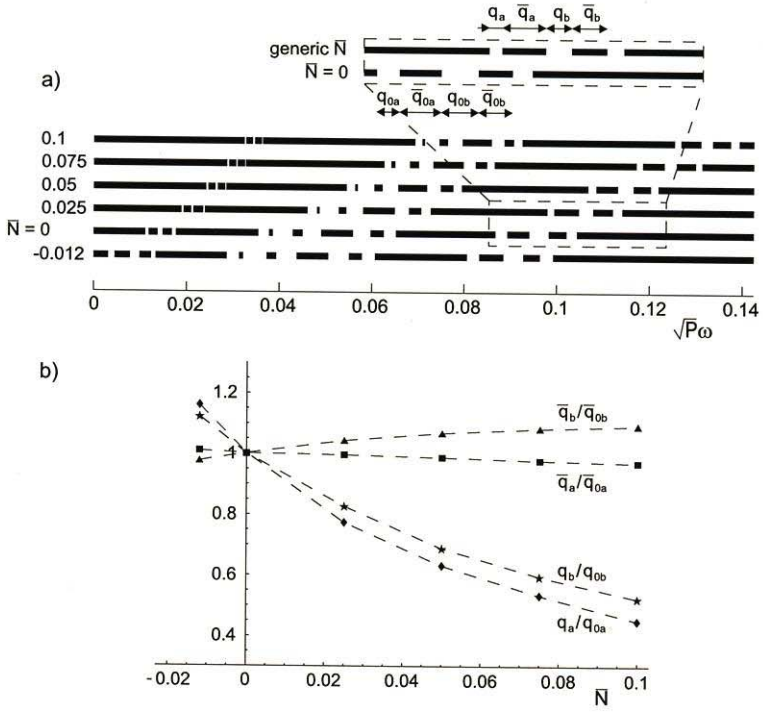

Fig. 3.13 (**a**) Effect of prestress $\overline{N}$ on stop/pass band distribution for flexural waves of a multi-supported quasiperiodic beam generated by sequence F_4; (**b**) influence of $\overline{N}$ on pass-band widths (represented by quantities q_1/q_{01}, q_2/q_{02}) and on stop-band widths (represented by quantities $\bar{q}_1/\bar{q}_{01}$, $\bar{q}_2/\bar{q}_{02}$). Subscript '0' denotes values for $\overline{N} = 0$. Reprinted from [10] with permission from Elsevier

can be easily obtained imposing $\omega = 0$ in (3.33) and treating N as the eigenvalue of (3.43).[1]

In Fig. 3.13(a), the stop/pass band distribution of a beam generated by sequence F_4 as functions of the axial load $\overline{N}$ (for $\sqrt{P}\omega < 0.1421$) is reported. Six values of $\overline{N}$ are investigated: $\overline{N} = -0.012$, a value slightly lower in absolute value than the buckling load, that corresponds to $\overline{N}_{buckl} = -0.01304$ (see footnote 1), $\overline{N} = 0, 0.025, 0.05, 0.075$, and 0.1. It is clear that a tensile stress shifts toward higher frequencies the bands, almost in a linear fashion, while in compression they move to lower frequencies, similarly to the problem analyzed in the previous section. Here it has been verified that no band-gap annihilation occurs.

The axial load has also an influence on the width of stop/pass bands. In Fig. 3.13(b), the stop/pass bands that in part (a) lie within the range $0.08 < \sqrt{P}\omega <$

[1] In terms of generation sequence F_i dimensionless buckling loads are $\overline{N}_{buckl}(F_0) = -0.03553$, $\overline{N}_{buckl}(F_1) = -0.00888$, $\overline{N}_{buckl}(F_2) = -0.01579$, $\overline{N}_{buckl}(F_3) = -0.01233$, $\overline{N}_{buckl}(F_4) = -0.01305$, $\overline{N}_{buckl}(F_5) = -0.01269$, $\overline{N}_{buckl}(F_6) = -0.01276$.

0.11 for $\overline{N} = 0$ (see the inset in Fig. 3.13(a)) are investigated. In particular, the ratios between their widths at different $\overline{N}$ and that at $\overline{N} = 0$ are reported in the plot. We note that stop-band widths (see the behaviour of ratios $\bar{q}_a/\bar{q}_{0a}$, $\bar{q}_b/\bar{q}_{0b}$) are weakly influenced by the prestress, while pass bands reduce (increase) considerably their lengths when a tensile (compressive) stress is applied (see q_a/q_{0a}, q_b/q_{0b}).

Acknowledgements M.G. and M.B. gratefully acknowledge the support of Italian Ministry of Education, University and Research (PRIN grant No. 2009XWLFKW); D.B. and A.B.M. gratefully acknowledge the support from the European Union FP7 under contract No. PIAP-GA-2011-286110-INTERCER2.

References

1. Aynaou, H., El Boudouti, E.H., Djafari-Rouhani, B., Akjouj, A., Velasco, V.R.: Propagation and localization of acoustic waves in Fibonacci phononic circuits. J. Phys. Condens. Matter **17**, 4245–4262 (2005)
2. Bacon, M.D., Dean, P., Martin, J.L.: Proc. Phys. Soc. **80**, 174 (1962)
3. Bigoni, D., Capuani, D., Bonetti, P., Colli, S.: A novel boundary element approach to time-harmonic dynamics of incremental non-linear elasticity: The role of pre-stress on structural vibrations and dynamic shear banding. Comput. Methods Appl. Mech. Eng. **196**, 4222 (2007)
4. Bigoni, D., Capuani, D.: Time-harmonic Green's function and boundary integral formulation for incremental nonlinear elasticity: Dynamics of wave patterns and shear bands. J. Mech. Phys. Solids **53**, 1163 (2005)
5. Bigoni, D., Gei, M., Movchan, A.B.: Dynamics of a prestressed stiff layer on an elastic half space: filtering and band gap characteristics of periodic structural models derived from long-wave asymptotics. J. Mech. Phys. Solids **56**, 2494–2520 (2008)
6. Chen, A.L., Wang, Y.S.: Study on band gaps of elastic waves propagating in one-dimensional disordered phononic crystals. Physica B **392**, 369–378 (2007)
7. Cremer, L., Leilich, H.O.: Zur theorie der biegekettenleiter. Arch. Elektr. Übertrag. **7**, 261 (1953)
8. Feynman, R.: The Feynman Lectures on Physics, vol. 2. Addison-Wesley, Reading (1965)
9. Gei, M.: Elastic waves guided by a material interface. Eur. J. Mech. A, Solids **27**, 328–345 (2008)
10. Gei, M.: Wave propagation in quasiperiodic structures: Stop/pass band distribution and prestress effects. Int. J. Solids Struct. **47**, 3067–3075 (2010)
11. Gei, M., Bigoni, D., Franceschini, G.: Thermoelastic small-amplitude wave propagation in nonlinear elastic multilayer. Math. Mech. Solids **9**, 555–568 (2004)
12. Gei, M., Movchan, A.B., Bigoni, D.: Band-gap shift and defect induced annihilation in prestressed elastic structures. J. Appl. Phys. **105**, 063507 (2009)
13. Gei, M., Ogden, R.W.: Vibration of a surface-coated elastic block subject to bending. Math. Mech. Solids **7**, 607–629 (2002)
14. Gurtin, M.E., Murdoch, A.I.: A continuum theory of elastic material surfaces. Arch. Ration. Mech. Anal. **57**, 291–323 (1975)
15. Hladky-Hennion, A.-C., Vasseur, J., Dubus, B., Djafari-Rouhani, B., Ekeom, D., Morvan, B.: J. Appl. Phys. **104**, 094206 (2008)
16. Hou, Z., Wu, F., Liu, Y.: Acoustic wave propagating in one-dimensional Fibonacci binary composite systems. Physica B **344**, 391–397 (2004)
17. John, S.: Strong localization of photons in certain disordered dielectric superlattices. Phys. Rev. Lett. **58**, 2486–2489 (1987)
18. King, P.D.C., Cox, T.J.: Acoustic band gaps in periodically and quasiperiodically modulated waveguides. J. Appl. Phys. **102**, 014908 (2007)

19. Kohmoto, M., Kadanoff, L.P., Tang, C.: Localization problem in one dimension: Mapping and escape. Phys. Rev. Lett. **50**, 1870–1872 (1983)
20. Kohmoto, M., Oono, Y.: Cantor spectrum for an almost periodic Schroedinger equation and a dynamical map. Phys. Lett. A **102**, 145–148 (1984)
21. Kohmoto, M., Sutherland, B., Iguchi, K.: Localization in optics: Quasiperiodic media. Phys. Rev. Lett. **58**, 2436–2438 (1987)
22. Kushwaha, M.S., Halevi, P., Dobrzynski, L., Djafari-Rouhani, B.: Acoustic band structure of periodic elastic composites. Phys. Rev. Lett. **71**, 2022–2025 (1993)
23. Lin, Y.K.: Free vibrations of a continuous beam on elastic supports. Int. J. Mech. Sci. **4**, 409–423 (1962)
24. Liu, Z., Chan, C. T, Sheng, P.: Analytic model of phononic crystals with local resonances. Phys. Rev. B **71**, 014103 (2005)
25. Liu, Z., Zhang, W.: Bifurcation in band-gap structures and extended states of piezoelectric Thue-Morse superlattices. Phys. Rev. B **75**, 064207 (2007)
26. Mead, D.J.: Wave propagation in continuous periodic structures: Research contributions from Southampton. J. Sound Vib. **190**, 495 (1996)
27. Mead, D.J.: Wave propagation and natural modes in periodic systems. II. Multi-coupled systems, with and without damping. J. Sound Vib. **40**, 19 (1975)
28. Miles, J.W.: Vibrations of beams on many supports. J. Eng. Mech. **82**, 1–9 (1956)
29. Milton, G.W., Willis, J.R.: On modifications of Newton's second law and linear continuum elastodynamics. Proc. R. Soc. Lond. A **463**, 855 (2007)
30. Movchan, A.B., Slepyan, L.I.: Band gap Green's functions and localized oscillations. Proc. R. Soc. Lond. A **463**, 2709 (2007)
31. Ogden, R.W., Steigmann, D.J.: Plane strain dynamics of elastic solids with intrinsic boundary elasticity, with application to surface wave propagation. J. Mech. Phys. Solids **50**, 1869–1896 (2002)
32. Page, J.H., Sukhovich, A., Yang, S., Cowan, M.L., Van Der Biest, F., Tourin, A., Fink, M., Liu, Z., Chan, C.T., Sheng, P.: Phys. Status Solidi B **241**, 3454 (2004)
33. Parnell, W.J.: Effective wave propagation in a prestressed nonlinear elastic composite bar. IMA J. Appl. Math. **72**, 223–244 (2007)
34. Pendry, J.B.: Negative refraction makes a perfect lens. Phys. Rev. Lett. **85**, 3966 (2000)
35. Sheng, P., Zhang, X.X., Liu, Z., Chan, C.T.: Physica B **338**, 201 (2003)
36. Sigalas, M.M., Economou, E.N.: Elastic and acoustic-wave band-structure. J. Sound Vib. **158**, 377–382 (1992)
37. Steigmann, D.J., Ogden, R.W.: Plane deformations of elastic solids with intrinsic boundary elasticity. Proc. R. Soc. Lond. A **453**, 853–877 (1997)
38. Timoshenko, S.P., Weaver, W., Young, D.H.: Vibration Problems in Engineering. Wiley, New York (1974)
39. Yablonovitch, E.: Inhibited spontaneous emission in solid-state physics and electronics. Phys. Rev. Lett. **58**, 2059–2062 (1987)
40. Yang, S., Page, J.H., Liu, Z., Cowan, M.L., Chan, C.T., Sheng, P.: Phys. Rev. Lett. **93**, 024301 (2004)
41. Zhang, X., Liu, Z.: Appl. Phys. Lett. **85**, 341 (2004)